Research Square

Preprints are preliminary reports that have not undergone peer review.
They should not be considered conclusive, used to inform clinical practice,
or referenced by the media as validated information.

Loosely Crosslinked Liquid Crystal Elastomers of High Compliance with Prolonged Creep Lifetime

Robert J. Chambers
University of California, San Diego
Marcus Wu
University of California, San Diego
Tyler Woodard
University of California, San Diego
Richey Li
University of California, San Diego
David Liu
University of California, San Diego
Raja Annapooranan
University of California, San Diego
Shengqiang Cai
s3cai@ucsd.edu

University of California, San Diego

Article

Keywords: liquid crystal elastomers, creep lifetime, creep rupture, crosslinked polymer networks, pressure-sensitive adhesives

Posted Date: June 16th, 2026

DOI: https://doi.org/10.21203/rs.3.rs-9931294/v1

License: This work is licensed under a Creative Commons Attribution 4.0 International License.
Read Full License

Additional Declarations: No competing interests reported.

Abstract

Polymeric elastomers subjected to a constant load exhibit time-dependent deformation known as creep. At low loads, the deformation gradually approaches an equilibrium state, whereas at higher loads, rupture occurs after a finite time, a phenomenon known as delayed fracture or static fatigue. The time to rupture decreases with increasing load and, for most elastomers, also diminishes with increasing compliance. However, many engineering applications—such as pressure-sensitive adhesives and sealing elastomers—require materials that simultaneously exhibit high compliance and long creep lifetimes, a combination that remains difficult to achieve. Here, we report that loosely crosslinked liquid crystal elastomers (LCEs) exhibit an unusual combination of high compliance and exceptional creep lifetime. The LCEs outperform a wide range of benchmark elastomers despite their high creep compliance.

1. Introduction

Soft elastomers are widely used in applications that require materials to deform easily while maintaining mechanical stability under load. In pressure-sensitive adhesives, sealing materials, wearable interfaces, and other load-bearing systems that require soft materials, high compliance is essential because it allows the material to conform to rough or uneven surfaces, increase real contact area, and reduce stress concentration at the interface.[1−4] For adhesive applications in particular, softness promotes surface wetting and tack, both of which are critical for strong initial adhesion.[5−8] However, these same applications also demand resistance to failure under sustained load. Typically, softer materials fail on shorter timescales, either by adhesive debonding from the substrate or by cohesive rupture after prolonged loading. Thus, an unusual but highly desirable combination for many soft material applications is high compliance together with long creep lifetime.[9]

Achieving this combination remains a major challenge in elastomer design. In covalently crosslinked polymer networks, reducing crosslink density is a common strategy to increase softness and deformability, provided the system remains above the gelation threshold. This relationship holds broadly across step-growth and chain-growth networks, although the specific network structure and defect distribution may influence the extent of the effect. This design space enables loosely crosslinked elastomers to achieve the low modulus needed for conformability and effective interfacial contact.[10]

Yet this gain in compliance is usually accompanied by a loss in mechanical stability under sustained stress.[11] Under a constant load, elastomers exhibit creep, a time-dependent increase in deformation that may eventually lead to rupture.[12] At relatively low loads, deformation can gradually approach an apparent equilibrium state, but at higher loads, creep rupture may occur after a finite time. In most conventional elastomers, time to rupture decreases as applied load increases, and it also tends to decrease as the material becomes more compliant.[13] This trade-off places an important limitation on the design of soft adhesives and other compliant structural elastomers.

This issue is especially important in pressure-sensitive adhesive systems. Pressure-sensitive adhesives must be soft enough to rapidly wet a substrate using only light applied pressure, but they must also maintain adhesion and resist creep failure during service.[14–17] These competing requirements are central to PSA performance. Materials that are too stiff may fail to form sufficient interfacial contact, while materials that are too soft may deform excessively and fracture.[18,19] As a result, the ability to combine softness with prolonged creep lifetime is a outstanding materials challenge in adhesive science. Similar considerations also apply to soft sealing components and compliant interfacial layers, where long-term performance depends not only on initial deformability but also on potential rupture under sustained load.

Conventional elastomers provide a useful benchmark for understanding this challenge. In polydimethylsiloxane (PDMS) networks, decreasing crosslink density lowers modulus and increases compliance, but it also accelerates creep and shortens creep lifetime.[20,21] Commercially available soft elastomeric adhesives often face the same basic limitation. Although these materials are engineered to be soft and tacky, their creep lifetime can remain insufficient for applications that require conformability and long-term load-bearing stability.[14,22–24] Consequently, new soft material platforms are needed that can escape the conventional coupling between compliance and creep lifetime.

Liquid crystal elastomers (LCEs) may offer such a route.[4,25–29] LCEs combine the elasticity of a polymer network with the orientational order of liquid crystalline mesogens, giving rise to unusual mechanical behavior not found in ordinary rubbers.[30] Their hierarchical structure enables deformation mechanisms such as soft elasticity and strain-induced alignment, which can produce high compliance at small to medium deformation while allowing greater stiffness increase as strain develops.[31–33] This distinctive response suggests that LCEs could provide a unique combination of compliance and creep lifetime under sustained loading. Although LCEs have been widely studied for actuation, adaptive surfaces, damping, and other responsive applications, their long-term creep rupture behavior as loosely crosslinked soft networks remains largely unexplored.[34–36]

In this study, we hypothesize that loosely crosslinked LCEs can overcome the conventional trade-off between compliance and creep lifetime. We compare the creep behavior of LCE networks with three crosslink densities against PDMS networks of comparable crosslink density as well as three commercially available soft elastomer materials. Creep rupture experiments were performed under constant load at a prescribed nominal stress. Both compliance and lifetime were evaluated across the full set of materials. We show that loosely crosslinked LCEs exhibit an unusual combination of high compliance and prolonged creep lifetime. In particular, the 3% crosslinked LCE displays creep lifetime that substantially exceeds that of PDMS and the commercial soft elastomer benchmarks despite its higher compliance. These results establish loosely crosslinked LCEs as a promising materials platform for applications that demand high softness and prolonged time to creep failure.

2. Results and Discussion

2.1 Hypothesis of high compliance and long creep lifetime in LCE

The central premise of this work is that LCEs may overcome the conventional trade-off between compliance and creep lifetime through their distinct network architecture and deformation mechanism. As illustrated schematically in Fig. 1A, the LCEs used consist of mesogenic units incorporated into a lightly crosslinked polymer network. Unlike conventional elastomers, this hierarchical structure introduces orientational degrees of freedom that can accommodate deformation through mesogen rotation without increasing the free energy of the system.[32,37] Consequently, LCEs are expected to exhibit a compliant response at small to moderate deformation while developing greater stiffness as alignment proceeds.

This concept is illustrated in Fig. 1B, which depicts the characteristic mechanical response associated with soft elasticity. Under load, the network can initially deform at relatively low stress through the rotation of liquid crystal mesogens, giving rise to a broad stress plateau. At larger deformation, mesogens align along the loading direction and the material undergoes pronounced strain stiffening. Such a response is attractive for load-bearing applications that require soft materials because it suggests a route to combine easy initial deformation, which promotes conformability and contact formation, with increased stiffness as strain develops, which may help delay creep rupture. In addition, the orientational order of the mesogens may alter the local fracture path by promoting crack deflection as damage develops, thereby providing another mechanism by which LCE architecture can influence failure, illustrated in Fig. 1C.[38] The chemical composition used to realize this behavior is shown in Fig. 1D, consisting of the liquid crystalline monomer RM257, the dithiol spacer EDDET, and the tetrafunctional crosslinker PETMP.

To test whether this molecular and mechanical design translates into improved long-term load-bearing performance, a custom constant-load creep platform was developed, as shown in Fig. 2. Individual specimens were suspended vertically between binder clips and loaded by dead weights, enabling sustained tensile loading under well-defined nominal stress (Fig. 2A). Multiple samples could be tested simultaneously in the custom-built frame, while a camera positioned normal to the sample plane recorded deformation for determining strain and creep lifetime (Fig. 2B). This setup enabled direct comparison of strain evolution, creep lifetime, and compliance across PDMS, LCEs, and commercial elastomer systems under identical loading conditions. Additional details of the setup are provided in the Experimental Methods Section.

It is important to note that though traditional adhesion tests were not performed in this study, the uniaxial tensile behavior of the elastomers is directly relevant to their adhesive performance. During debonding between an adhesive and a substrate, fibrils commonly form and are subjected to uniaxial tension; consequently, the mechanical response measured under uniaxial loading directly governs how these fibrils deform and ultimately fail.[29] Several previous models have established quantitative links

between the stress–strain response of an adhesive elastomer and its macroscopic adhesion performance, further supporting the relevance of this testing geometry for adhesive applications.[5]

With this framework established, we first examined the uniaxial tensile behavior of the materials to determine how liquid-crystalline network architecture alters the balance between stiffness, strain stiffening, and extensibility before evaluating their constant-load creep response.

2.2 Uniaxial Tensile Properties

Figure 3 compares the uniaxial tensile behavior of Sylgard 184 PDMS networks and LCEs with varying crosslink density. For the PDMS samples, the Sylgard 184 A:B ratio refers to the mass ratio of base polymer to curing agent, where lower A:B ratios correspond to higher curing-agent content and therefore higher effective crosslink density; additional details on sample preparation are provided in the Experimental Methods section. As expected, the PDMS samples exhibited the typical trade-off between stiffness and extensibility with increasing curing-agent content (Fig. 3A).[21] All replicates are shown in **Figure S1.** A summary of the tensile properties and associated standard deviations are provided in **Table S1.** The 15:1 formulation showed the highest initial stiffness and reached the greatest stress at a given strain, whereas the 30:1 formulation was substantially softer and carried much lower stress throughout deformation. Based on the slope of the secant line connecting 0% and 100% strain in the stress strain curve, the secant modulus of the PDMS increased from 0.03 MPa for the 30:1 formulation to about 0.09, 0.15, and 0.25 MPa for the 25:1, 20:1, and 15:1 formulations, respectively. These results confirm that decreasing the base-to-curing-agent ratio increased the effective crosslink density and produced a progressively stiffer network response.

The LCEs exhibited a markedly different tensile response (Fig. 3B, C). Crosslink ratio is defined here as the molar ratio of PETMP to EDDET; for example, the 3% crosslinked LCE corresponds to an RM257/EDDET/PETMP molar ratio of 100/97/3, with additional formulation details provided in the Experimental Methods. All replicates are shown in **Figure S2**. After an initially stiffer response over approximately 0–20% strain, all LCE compositions entered a more compliant regime, with secant moduli of 0.064 MPa for the 3% crosslinked LCE, 0.103 MPa for the 6% crosslinked LCE, and 0.126 MPa for the 9% crosslinked LCE, calculated from 0–100% strain. All three LCE formulations exhibited a stress plateau over approximately 20–120% strain that is characteristic of soft elasticity. At larger deformation, however, the LCEs displayed pronounced strain stiffening. This effect became stronger as crosslink density increased, with the 9% crosslinked LCE showing the earliest and most rapid increase in stress, followed by the 6% and then the 3% LCE. All three LCE formulations fractured at a nominal stress level around 1.75 MPa. In terms of extensibility, all PDMS samples fractured below 200% strain, whereas the LCEs sustained much larger deformations before failure, with the 3% crosslinked LCE extending beyond 1200% strain. The 6% and 9% crosslinked LCE failed at approximately 625% and 450% strain, respectively.

Since these tensile properties are intended to inform creep performance, we next compared the LCEs against soft commercial adhesive elastomers that similarly rely on compliance for contact formation but

must also resist creep failure under sustained load. The commercial soft elastomer benchmarks spanned a broad range of tensile responses (**Figure S3**). Among the three commercial materials, Scotch 15 (3M 410H-MED-DC) exhibited the steepest initial stress increase, corresponding to a secant modulus of 0.272 MPa, and failed at a relatively low strain of approximately 300%, indicating the stiffest and least extensible response. By contrast, VHB 4910 (3M VHB™ 4910) and Scotch 20 (3M Scotch-Mount™ Multipurpose Gel Tape) were softer and more extensible, with secant moduli of 0.098 and 0.080 MPa, respectively, and failed at substantially larger strains of approximately 800% and 960%, while both reached maximum stresses near 0.4 MPa. Relative to commercial materials, the LCEs combined similar extensibility with a more distinctive soft-elastic plateau followed by a strain stiffening regime at the strain rate of 0.1 s^{-1}.

Based on the tensile results, the selected PDMS formulations and commercial adhesive elastomers provide relevant benchmarks for evaluating how soft elasticity, induced by mesogenic reorientation, influences creep compliance and lifetime in LCE networks. However, uniaxial tension alone cannot determine how these materials perform under sustained load. Next, we performed constant-load creep experiments to determine whether the distinctive tensile response of LCEs translates into improved creep lifetime relative to PDMS and the commercial elastomer benchmarks.

2.3 Creep Behavior of Lightly Crosslinked Elastomers

Figure 4 compares the constant-load creep response of PDMS and LCE networks at applied nominal stresses of 0.09, 0.14, and 0.19 MPa. Across all conditions, the two material classes exhibited fundamentally different behavior. The PDMS samples deformed only modestly under load, but their creep lifetime decreased sharply as stress increased, especially for the softer formulations as shown in Fig. 5. By contrast, the LCEs sustained substantially larger creep strains while remaining intact for much longer times, indicating that high compliance in these networks does not come at the usual expense of creep durability. LCEs appear to follow a different deformation pathway under load, consistent with soft elasticity followed by alignment-induced reinforcement.[32] For specimens that survived the experimental cutoff, the reported lifetime represents a lower bound rather than the true creep failure time.

At 0.09 MPa, all PDMS formulations quickly deformed to an initial strain and then underwent only slight additional creep over time (Fig. 4A), consistent with a predominantly elastic response followed by limited time-dependent deformation. The maximum strain decreased with increasing crosslink density. The 30:1 sample failed in less than 140 seconds at strains near 200%. The 25:1, 20:1, and 15:1 sustained strain of approximately 50%, 40%, and 15%, respectively. The LCEs responded very differently (Fig. 4D). All three formulations underwent a large initial deformation followed by continued slow creep over hundreds of hours, and the magnitude of strain increased strongly with decreasing crosslink density. The 3% LCE reached strains on the order of 1000%, far exceeding both the 6% and 9% LCEs and all PDMS, remaining intact for the duration of the two-week experiment. LCE 6% and LCE 9% reached strains of 200% and 100%, respectively. Even at the lowest applied stress, the LCEs exhibited a markedly different combination of deformability and creep stability compared to PDMS.

This contrast became even more pronounced at 0.14 MPa. The PDMS samples again showed relatively small creep strain, but their lifetimes were substantially reduced, particularly for the softer formulations (Fig. 4B). The creep failure times for 30:1, 25:1 and 20:1 were 10 s, 24 s and 1190 s, respectively. The 15:1 formulation reached the experimental cutoff intact. In contrast, the LCEs again combined substantially larger creep strain with substantially longer survival (Fig. 4E). All three formulations maintained much larger strain than PDMS while surviving for substantially longer times. Most notably, the 3% LCE deformed to strains above 1000% while still approaching the experimental cutoff. Even the 6% and 9% LCEs, although much less deformable than the 3% formulation, maintained larger creep deformation than PDMS together with longer lifetimes. LCE 6% and LCE 9% reached strains of 300% and 130%, respectively.

At 0.19 MPa, the divergence between the two material classes was most evident. The PDMS response became strongly lifetime-limited: the softer formulations failed almost immediately (Fig. 4C). Once the applied stress entered this higher regime, PDMS could no longer accommodate deformation without rapid rupture. The LCEs showed the opposite behavior (Fig. 4F). The 3% LCE reached the largest strain of all materials and failed only after strains above 1000% in around 150 h, whereas the 6% LCE sustained strains around 450% with an average creep lifetime of 114 h, and the 9% LCE remained at comparatively low strain around 200% while surviving the experimental cutoff. Thus, although increasing LCE crosslink density reduced creep strain, all three LCE formulations retained substantially greater deformation capacity than PDMS and retained much longer lifetime.

The short-time creep compliance data further emphasize the unusual mechanical regime of the LCEs. Creep compliance, $J(t)$, was calculated as the time-dependent strain divided by the constant applied nominal stress, $J(t) = \epsilon(t)/\sigma_0$, where $\epsilon(t)$ is the measured strain and σ_0 is the applied nominal stress level. In PDMS (Fig. 5G), creep compliance remained relatively low and varied only modestly over the first several hours, with the more lightly crosslinked networks showing greater compliance as expected. However, the absolute compliance values remained small, reflecting the limited creep strain observed in Fig. 4. PDMS 30:1 had the maximum compliance of all PDMS formulations with a compliance of 22 MPa^{-1} at 1 min. Any PDMS sample that did not fail in less than 1 h has creep compliance below 5 MPa^{-1}. By contrast, the LCEs exhibited much larger creep compliance, especially at low crosslink density (Fig. 5H). LCE 3% showed by far the highest compliance and continued to increase over time, while the 6% and 9% LCEs also exceeded the PDMS values despite their longer lifetimes. The creep compliance for LCE 3% was between 50–80 MPa^{-1} in the 1–5 h range. LCE 6% and LCE 9% had creep compliance around 20 and 10 MPa^{-1} during this time range. These results show that the improved lifetime of the LCEs is not achieved by suppressing deformation. Rather, the LCEs remain highly compliant while simultaneously resisting premature creep rupture.

To place these results in a more application-relevant context, we compared the creep properties of the LCEs with three commercially available soft elastomeric tapes: VHB, Scotch 15, and Scotch 20. Before comparing directly with the LCEs, we note that a tradeoff between compliance and creep lifetime is evident within the PDMS formulations, where more compliant formulations exhibited shorter creep

lifetimes. A similar tradeoff appears again across the three commercial adhesive elastomers. Figure 6A–C shows the creep response of these materials at applied stresses of 0.09, 0.14, and 0.19 MPa. At 0.09 MPa, Scotch 20 showed the largest strain, rising rapidly to values near 800%, while VHB reached strains of about 450% and Scotch 15 remained lower, around 250%. These strain levels are comparable to those of the LCE 3%, 6% and 9% respectively; however, the creep lifetimes were substantially different, with all LCE materials remaining intact and all commercial materials failing well before the experimental cutoff. The creep lifetime at 0.09 MPa was less than 5 h, 10 h, and 200 h for Scotch 20, VHB and Scotch 15, respectively. At 0.14 MPa, the distinction in creep lifetime became even clearer: all three commercial tapes deformed rapidly and failed far sooner than the LCEs, with Scotch 20 again showing the fastest and largest deformation, failing in less than 1 h, VHB failed in less than 2 h at strains around 600%, and Scotch 15 failed in less than 5 h at strains around 400%. At 0.19 MPa, the same overall trend persisted but on still shorter timescales. All three commercial materials underwent rapid deformation and failure in less than 0.3 h. Thus, in PDMS and across commercial adhesive elastomers, higher compliance is generally associated with shorter creep lifetime. In contrast, the LCEs reached maximum strains comparable to those of the commercial tapes while maintaining substantially longer creep lifetimes.

The Ashby plots in Fig. 6D–F place the materials within a broader performance landscape by comparing creep compliance and creep failure lifetime across all three stress levels at two representative time points, 5 min and 2 h. At each applied stress, the 5 min and 2 h compliance values, denoted as $J(t = 5\,\mathrm{min})$ and $J(t = 2\,\mathrm{h})$, show how each material evolves during sustained loading. The 5 min compliance values are plotted with solid markers, while the 2 h compliance values are plotted with empty markers, allowing the early deformation response and subsequent evolution of compliance under sustained loading to be compared directly. At each applied stress, the PDMS formulations cluster in a low-compliance regime, whereas the commercial tapes occupy a high-compliance, short-lifetime regime. The LCEs lie between these two extremes in compliance, but importantly not as a simple average between them. Instead, they extend into a distinct region characterized by high creep compliance together with prolonged failure lifetime. This feature is most pronounced for the 3% LCE, which consistently reaches compliance values comparable to the commercial elastomer tapes while maintaining lifetimes that are orders of magnitude longer. The 6% and 9% LCEs occupy adjacent regions of lower compliance but similarly long lifetime, together defining a property space that is not accessed by either PDMS or the commercial adhesive benchmarks alone.

Comparing the 5 min and 2 h compliance values further highlight important differences in time-dependent deformation across material classes. In the PDMS samples, the 5 min and 2 h creep compliance values largely overlap because the compliance changes only weakly over this interval. In contrast, in the more viscous commercial materials and LCEs, the creep compliance increases from 5 min to 2 h. Overall, these plots show that the loosely crosslinked LCEs overcome the conventional compliance-lifetime trade-off that constrains model silicone elastomers and commercial soft adhesive materials. The decoupling of compliance from poor load-bearing durability suggests that the superior creep lifetime of LCEs arises not simply from network stiffness, but from a distinct deformation and failure pathway enabled by liquid-crystalline mesogens.

An explanation for the balance of creep compliance and lifetime present in LCEs is that the mesogens in the LCE networks play two mechanical roles during creep. First, mesogen rotation enables soft elasticity at small to moderate strain. This mechanism allows the material to accommodate deformation through internal reorientation of liquid crystalline domains rather than immediately resisting deformation through conventional rubber-elastic stretching alone. As a result, the LCEs can remain relatively compliant despite being load-bearing.

Second, once deformation proceeds further, mesogen alignment appears to introduce a reinforcing mechanism that is absent in regular elastomers. The tensile results showed pronounced strain stiffening in the LCEs, with stress rising rapidly after the initial stress plateau. This transition likely reflects progressive alignment of mesogens and network strands along the loading direction. Such alignment can increase the stiffness of the network and may suppress the growth of defects.[39]

It is also noted that creep rupture usually occurs near microscopic flaws, where local stress concentrations promote crack growth.[40,41] In conventional elastomers such as PDMS, these flaws can gradually enlarge as the surrounding network undergoes progressive chain stretching, shown schematically in Fig. 1C. In contrast, LCEs provide an additional mechanism for resisting flaw growth. Near a crack tip, the local strain field can be much larger than the nominal applied strain, causing mesogens in the highly deformed region to rotate and align with the tensile direction.[39] This local mesogen alignment create a reinforced zone ahead of the crack tip, blunting the crack and delaying further propagation.[38,42] Thus, while the loosely crosslinked LCE network remains compliant enough to deform under load, its deformation-induced alignment can suppress defect growth and extend creep lifetime. This flaw-tolerance mechanism helps to explain why the LCEs survived much longer than PDMS and commercial soft elastomers under sustained stress, despite exhibiting high creep compliance. For PSA applications, this combination of compliance and resistance to flaw-driven rupture is especially valuable during fibril-dominated deformation, where local stress concentrations can otherwise accelerate debonding or cohesive failure.[29]

3. Conclusion

In summary, loosely crosslinked liquid crystal elastomers exhibit an unusual combination of high compliance and prolonged creep lifetime. Compared with PDMS and commercial soft adhesive benchmarks, the LCEs sustain much larger deformation while remaining intact for substantially longer under constant load. Most notably, the 3% crosslinked LCE combines very high creep compliance with creep lifetime that exceeds conventional elastomer networks and commercial pressure-sensitive adhesives.

These results show that softness and long-term load-bearing stability need not be mutually exclusive in lightly crosslinked polymer networks. The superior performance of the LCEs is attributed not simply to network stiffness, but to their distinctive deformation mechanism associated with the rotation of liquid crystal mesogens, which enables soft elasticity at small to moderate strain and progressive strain

stiffening at larger deformation. This deformation-dependent response likely delays damage accumulation and creep rupture under sustained load.

Taken together, the results identify loosely crosslinked LCEs as a promising materials platform for pressure-sensitive adhesives and other load-bearing applications that require conformability and long-term mechanical stability. Future work should directly probe the role of mesogen alignment during creep and extend these materials to practical adhesive interfaces and geometries. Existing creep models for conventional elastomers and pressure-sensitive adhesives provide a useful starting point for describing these viscoelastic materials.[17,23,24,43] Future constitutive models should incorporate both time-dependent viscoelastic relaxation and deformation-induced director/mesogen reorientation to capture the coupled compliance and delayed rupture behavior observed here.

4. Experimental Section/Methods

Materials

1,4-Bis-[4-(3-acryloyloxypropyloxy)benzoyloxy]-2-methylbenzene (RM257; Chemfish Japan; 97%), 2,2'-(ethylenedioxy)diethanethiol (EDDET; Sigma-Aldrich; 95%), pentaerythritoltetrakis(3-mercaptopropionate) (PETMP; Sigma-Aldrich; 95%), dipropylamine (DPA; Sigma-Aldrich; 98%), butylated hydroxytoluene (BHT; 99% Sigma-Aldrich), and toluene (Fisher Scientific; 99%) were used as received without further purification. Sylgard™ 184 Silicone Elastomer Kit (Dow, Midland, MI, USA) was used to prepare the PDMS samples in this study. Commercial soft elastomeric tapes, including 3M VHB™ 4910, 3M 410H-MED-DC, and 3M Scotch-Mount™ Multipurpose Gel Tape, were commercially obtained and used as received. For clarity, these materials are hereafter referred to as VHB, Scotch 15, and Scotch 20, respectively.

LCE Synthesis: At room temperature (20°C), the LCEs investigated in this study were in a polydomain nematic state. The polydomain LCEs were synthesized through a Michael addition reaction using the acrylate-terminated liquid crystal monomer RM257, the thiol spacer EDDET, and the thiol crosslinker PETMP, with dipropylamine (DPA) as the catalyst, following a previously reported procedure.[44] RM257 (10 g, 16.98 mmol) and butylated hydroxytoluene (BHT, 0.1 g) were first dissolved in toluene (4 g) at 85°C, where BHT was used to suppress undesired crosslinking of the acrylate groups. EDDET and PETMP were then introduced to obtain molar ratios of RM257/EDDET/PETMP = 100/97/3, 100/94/6, and 100/91/9, corresponding to 3%, 6%, and 9% crosslinked LCEs, respectively. A diluted DPA solution (0.05 g, 0.49 mmol in toluene, 1:50 v/v) was then added, and the mixture was thoroughly stirred. The reaction mixture was degassed, cast into a covered glass mold, and cured at room temperature for 24 hours. After curing, the LCE films were removed from the mold and heated at 85°C to remove residual solvent.

PDMS Synthesis:

PDMS networks were prepared from the Sylgard™ 184 silicone elastomer kit by mixing the base and curing agent at mass ratios of 15:1, 20:1, 25:1, and 30:1. The mixtures were mixed using a Thinky planetary centrifugal mixer (ARE-310SCE) at 2000 rpm for 1 min, followed by degassing for 15 min to

remove entrapped air. The degassed silicone was then poured into a glass mold and cured at room temperature for 24 h. The cured samples were subsequently post-cured in an oven at 65°C for 2 h prior to testing.

Uniaxial Tension Testing:

Uniaxial tensile tests were performed to characterize the monotonic mechanical response of the elastomer samples. Rectangular specimens with a gauge length of 20 mm and width of 10 mm were prepared. To ensure reliable gripping and minimize slippage during testing, the ends of each specimen were bonded to acrylic plates that served as rigid gripping tabs. Tensile tests were conducted using an Instron 5965 equipped with a 1 kN load cell. Samples were loaded under displacement control at a constant strain rate of 0.1 s^{-1} until failure. For each material condition, three independent specimens were tested (n = 3), and the resulting stress–strain curves were used to assess tensile behavior.

Creep Experiment:

Rectangular specimens measuring 40 mm × 10 mm were cut from the elastomer sheets. A gauge region was defined by marking lines 10 mm from each end of the specimen using a permanent marker. Binder clips were attached at these marked positions so that the gripped regions remained outside the gauge length throughout the experiment. The specimen thickness was measured prior to testing, and the suspended mass required to achieve the desired applied stress was selected accordingly. Each specimen was then mounted vertically on a custom-built creep test frame, depicted in Fig. 2B, and the selected weight was attached to the lower binder clip to apply a constant load (Fig. 2A). These weights corresponded to stress levels of 0.09 MPa, 0.14 MPa, and 0.19 MPa. Stresses were calculated based on the sample cross-sections, with a width of 1 cm and the respective thickness of each material. A DSLR camera (Canon EOS Rebel T3i, equipped with an EF 24mm f/1.4L II USM lens) was positioned 140 cm from the fixture to capture the deformation of the samples during testing. With weights attached, the camera was set to take pictures every 5–30 s for the first five minutes to capture initial sample deformation. The exact capture rate depended on the expected lifetime of each specimen. After this, the capture rate was reduced to one picture every 10–30 min. The fixture allowed up to sixteen samples to be tested simultaneously. After testing, the image sequence for each specimen was analyzed using a custom MATLAB script that tracked two marker points located on the binder clips, extracted the image timestamps, and calculated the specimen strain as a function of time. Because the tracked points were located on the binder clips, the reported strain reflects the relative displacement between grips; specimens were visually inspected to ensure that grip slippage did not occur. For each material and stress condition, at least three independent specimens were tested unless otherwise noted.

Declarations

Acknowledgements

The authors acknowledge the support of the US Army Research Office under Grant No. W911NF-20-2-0182.

Author Contributions

R.J.C. designed the experiments, prepared samples, performed experiments, analyzed data, prepared figures, and wrote the original draft. M.W., T.W., and D.L. prepared samples, performed experiments, and contributed to data analysis. R.L. developed the image-analysis code used to quantify creep deformation. R.A. contributed to experimental design, data interpretation, project guidance, and manuscript revision. S.C. supervised the project, acquired funding, guided the overall research direction, and revised the manuscript. All authors reviewed and approved the final manuscript.

Competing Interests

The authors declare no financial or non-financial competing interests.

Data Availability Statement

The data that support the findings of this study are available from the corresponding author upon reasonable request. The custom MATLAB script used for image analysis is available from the corresponding author upon reasonable request.

References

1. King, D. R. & Crosby, A. J. Optimizing Adhesive Design by Understanding Compliance. *ACS Appl. Mater. Interfaces* **7**, 27771–27781 (2015).
2. Windslow, R. J. & Busfield, J. J. C. Viscoelastic modeling of extrusion damage in elastomer seals. *Soft Materials* **17**, 228–240 (2019).
3. Yuk, H. *et al.* Dry double-sided tape for adhesion of wet tissues and devices. *Nature* **575**, 169–174 (2019).
4. Annapooranan, R., Yeerella, R. H., Chambers, R. J., Li, C. & Cai, S. Soft elasticity enabled adhesion enhancement of liquid crystal elastomers on rough surfaces. *Proc. Natl. Acad. Sci. U.S.A.* **121**, e2412635121 (2024).
5. Gent, A. R. & Petrich, R. P. Adhesion of viscoelastic materials to rigid substrates. *Proc. R. Soc. A* **310**, 433–448 (1969).
6. Johnson, K. L., Kendall, K. & Roberts, A. D. Surface energy and the contact of elastic solids. *Proc. R. Soc. A* **324**, 301–313 (1971).
7. Zosel, A. Adhesion and Tack of Polymers: Influence of Mechanical Properties and Surface Tensions. *Colloid Polym. Sci.* **263**, 541–553 (1985).
8. Creton, C. & Leibler, L. How does tack depend on time of contact and contact pressure? *J. Polym. Sci. B Polym. Phys.* **34**, 545–554 (1996).

9. *Technology of Pressure-Sensitive Adhesives and Products*. (CRC Press, Boca Raton, FL, 2009).
10. Wang, Q. *et al.* Bulk and Interfacial Contributions to the Adhesion of Acrylic Emulsion-Based Pressure-Sensitive Adhesives. *Macromolecules* **53**, 6975–6983 (2020).
11. de Gennes, P. G. Soft Adhesives. *Langmuir* **12**, 4497–4500 (1996).
12. Findley, W., Lai, J. & Onaran, K. *Creep and Relaxation of Nonlinear Viscoelastic Materials*. (Dover Publications, New York, NY, 1976).
13. Plazek, D. J. Effect of crosslink density on the creep behavior of natural rubber vulcanizates. *J. Polym. Sci. A-2 Polym. Phys.* **4**, 745–763 (1966).
14. Townsend, B. W. *et al.* Characterizing acrylic foam pressure sensitive adhesive tapes for structural glazing applications—Part II: Creep rupture results. *Int. J. Adhes. Adhes.* **31**, 650–659 (2011).
15. Barquins, M. & Ciccotti, M. On the kinetics of peeling of an adhesive tape under a constant imposed load. *Int. J. Adhes. Adhes.* **17**, 65–68 (1997).
16. Deshpande, A., Song, Z. & Vaidya, S. A Creep Model For Pressure Sensitive Adhesives Under Shear Load. in *2020 Asia-Pacific International Symposium on Advanced Reliability and Maintenance Modeling (APARM)* 1–5 (IEEE, Vancouver, BC, Canada, 2020). doi:10.1109/APARM49247.2020.9209475.
17. Simões, B. D. *et al.* The role of competing timescales of viscoelastic stress redistribution and edge-initiated interfacial cracking in creep failure modes of pressure-sensitive adhesive joints. *J. Adhes.* 1–29 (2026) doi:10.1080/00218464.2026.2627462.
18. Gay, C. & Leibler, L. Theory of Tackiness. *Phys. Rev. Lett.* **82**, 936–939 (1999).
19. Hui, C. Y., Lin, Y. Y. & Baney, J. M. The mechanics of tack: Viscoelastic contact on a rough surface. *J. Polym. Sci. B Polym. Phys.* **38**, 1485–1495 (2000).
20. Nielsen, L. E. Cross-Linking–Effect on Physical Properties of Polymers. *Journal of Macromolecular Science, Part C* **3**, 69–103 (1969).
21. Darby, D. R., Cai, Z., Mason, C. R. & Pham, J. T. Modulus and adhesion of Sylgard 184, Solaris, and Ecoflex 00-30 silicone elastomers with varied mixing ratios. *J. Appl. Polym. Sci.* **139**, e52412 (2022).
22. Simões, B. D. *et al.* An Exploratory Study on Determining and Modeling the Creep Behavior of an Acrylic Pressure-Sensitive Adhesive. *Materials* **16**, 2029 (2023).
23. Fernandes, É. M. D. *et al.* Analytical model for static and cyclic creep behavior of pressure-sensitive adhesives. *Mechanics of Advanced Materials and Structures* **31**, 9426–9439 (2024).
24. Yao, L. *et al.* Anti-Creep Adhesive Tapes via Trapped-Entanglement-Regulated Topological Networks. *Advanced Materials* **38**, e13105 (2025).
25. Gou, H., Hou, S. & Saed, M. O. Strong, Reversible, Heat-Activated Adhesion from Liquid Crystal Polymer Networks. *Adv. Mater. Interfaces* **11**, 2400488 (2024).
26. Choi, S. *et al.* Harnessing Extreme Internal Damping in Polyrotaxane-Incorporated Liquid Crystal Elastomers for Pressure-Sensitive Adhesives. *Adv. Funct. Mater.* **35**, 2413824 (2025).

27. Koshimizu, N. & Saed, M. O. Switchable Pressure-Sensitive Adhesion in Nematic Side-Chain Liquid Crystal Elastomers. *Macromolecules* **58**, 12191–12200 (2025).
28. Farre-Kaga, H. J., Saed, M. O. & Terentjev, E. M. Dynamic Pressure Sensitive Adhesion in Nematic Phase of Liquid Crystal Elastomers. *Adv. Funct. Mater.* **32**, 2110190 (2022).
29. Annapooranan, R., Jeyakumar, S., Chambers, R., Long, R. & Cai, S. Ultra Rate-Dependent Pressure Sensitive Adhesives Enabled by Soft Elasticity of Liquid Crystal Elastomers. *Adv. Funct. Mater.* **34**, 2309123 (2024).
30. Warner, M. & Terentjev, E. M. Nematic elastomers—A new state of matter? *Prog. Polym. Sci.* **21**, 853–891 (1996).
31. Warner, M., Bladon, P. & Terentjev, E. M. "Soft elasticity" — deformation without resistance in liquid crystal elastomers. *J. Phys. II France* **4**, 93–102 (1994).
32. Ware, T. H., Biggins, J. S., Shick, A. F., Warner, M. & White, T. J. Localized soft elasticity in liquid crystal elastomers. *Nat. Commun.* **7**, 10781 (2016).
33. Tokumoto, H. *et al.* Probing the in-plane liquid-like behavior of liquid crystal elastomers. *Sci. Adv.* **7**, eabe9495 (2021).
34. He, Q., Wang, Z., Song, Z. & Cai, S. Bioinspired Design of Vascular Artificial Muscle. *Adv. Mater. Technol.* **4**, 1800244 (2019).
35. Babakhanova, G. *et al.* Liquid crystal elastomer coatings with programmed response of surface profile. *Nat. Commun.* **9**, 456 (2018).
36. Mistry, D. *et al.* Soft elasticity optimises dissipation in 3D-printed liquid crystal elastomers. *Nat. Commun.* **12**, 6677 (2021).
37. Merkel, D. R., Shaha, R. K., Yakacki, C. M. & Frick, C. P. Mechanical energy dissipation in polydomain nematic liquid crystal elastomers in response to oscillating loading. *Polymer* **166**, 148–154 (2019).
38. Guo, Q., Zhang, S. & Cai, S. Crack deflection in liquid crystal elastomers determined by energy release rate maximization: Experiments and simulations. *Eng. Fract. Mech.* **329**, 111602 (2025).
39. Lake, G. J. & Thomas, A. G. The Strength of Highly Elastic Materials. *Proceedings of the Royal Society of London. Series A, Mathematical and Physical Sciences* **300**, 108–119 (1967).
40. Rivlin, R. S. & Thomas, A. G. Rupture of rubber. I. Characteristic energy for tearing. *J. Polym. Sci.* **10**, 291–318 (1953).
41. Bonn, D., Kellay, H., Prochnow, M., Ben-Djemiaa, K. & Meunier, J. Delayed Fracture of an Inhomogeneous Soft Solid. *Science* **280**, 265–267 (1998).
42. Zhou, Y., Wei, C. & Jin, L. Fracture of liquid crystal elastomers. *Proc. Natl. Acad. Sci. U.S.A.* **122**, e2510727122 (2025).
43. Adibeig, M. R., Xue, Q. & Yang, C. Effects of network structure on the viscoelastic creep and delayed fracture of polyelectrolyte elastomers. *Polymer* **305**, 127104 (2024).
44. Yakacki, C. M. *et al.* Tailorable and programmable liquid-crystalline elastomers using a two-stage thiol–acrylate reaction. *RSC Adv.* **5**, 18997–19001 (2015).

Figures

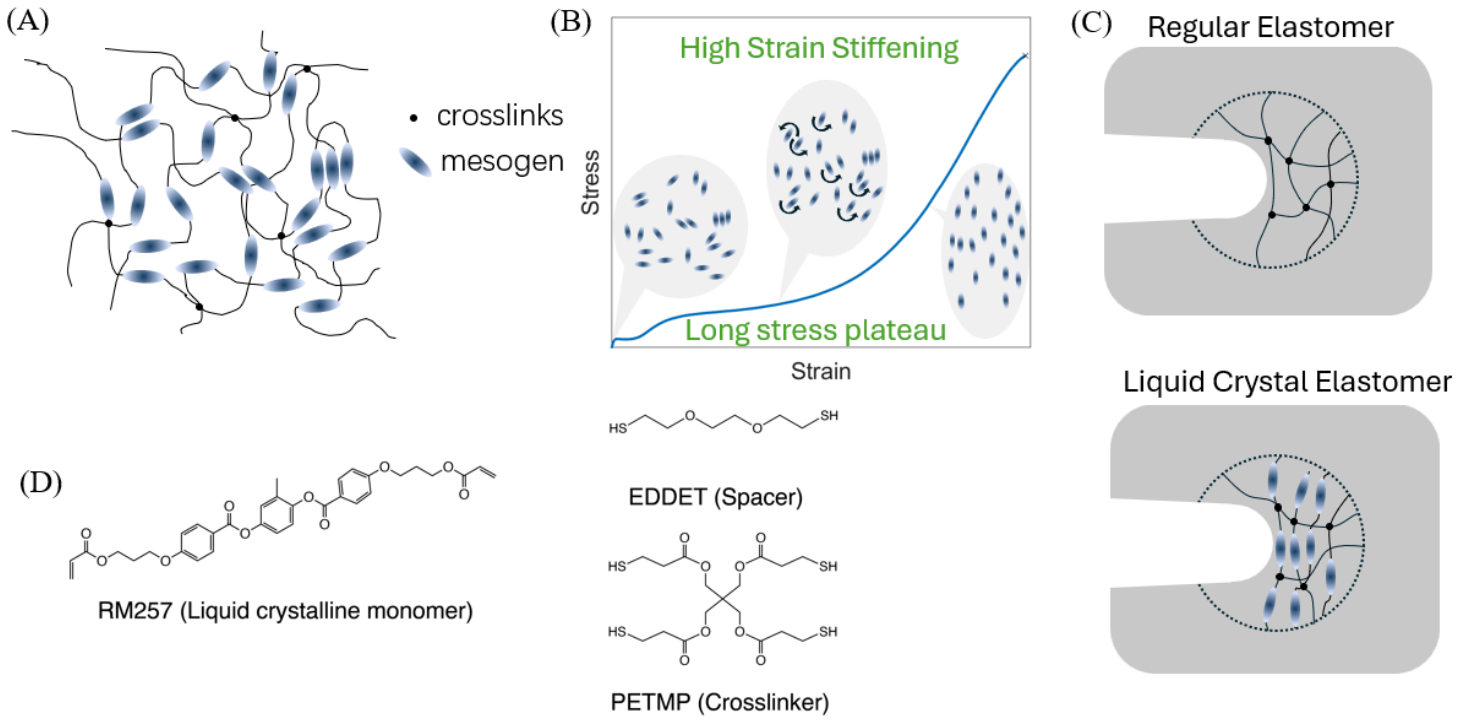


Figure 1

(A) Schematic representation of the crosslinked LCE network, consisting of mesogenic units incorporated into a lightly crosslinked polymer backbone that forms an elastomeric network. (B) Illustration of soft elasticity in the LCE, where applied strain induces mesogenic rotation and director reorientation, enabling large deformation at relatively low stress. (C) Schematic comparison of crack growth in a regular elastomer and a liquid crystal elastomer. In the LCE, mesogen alignment and reorientation near the crack tip may redistribute deformation, promote crack-tip blunting, and deflect the crack path. (D) Chemical structures of the LCE system used in this study, showing the mesogenic monomer, crosslinker, and spacer.

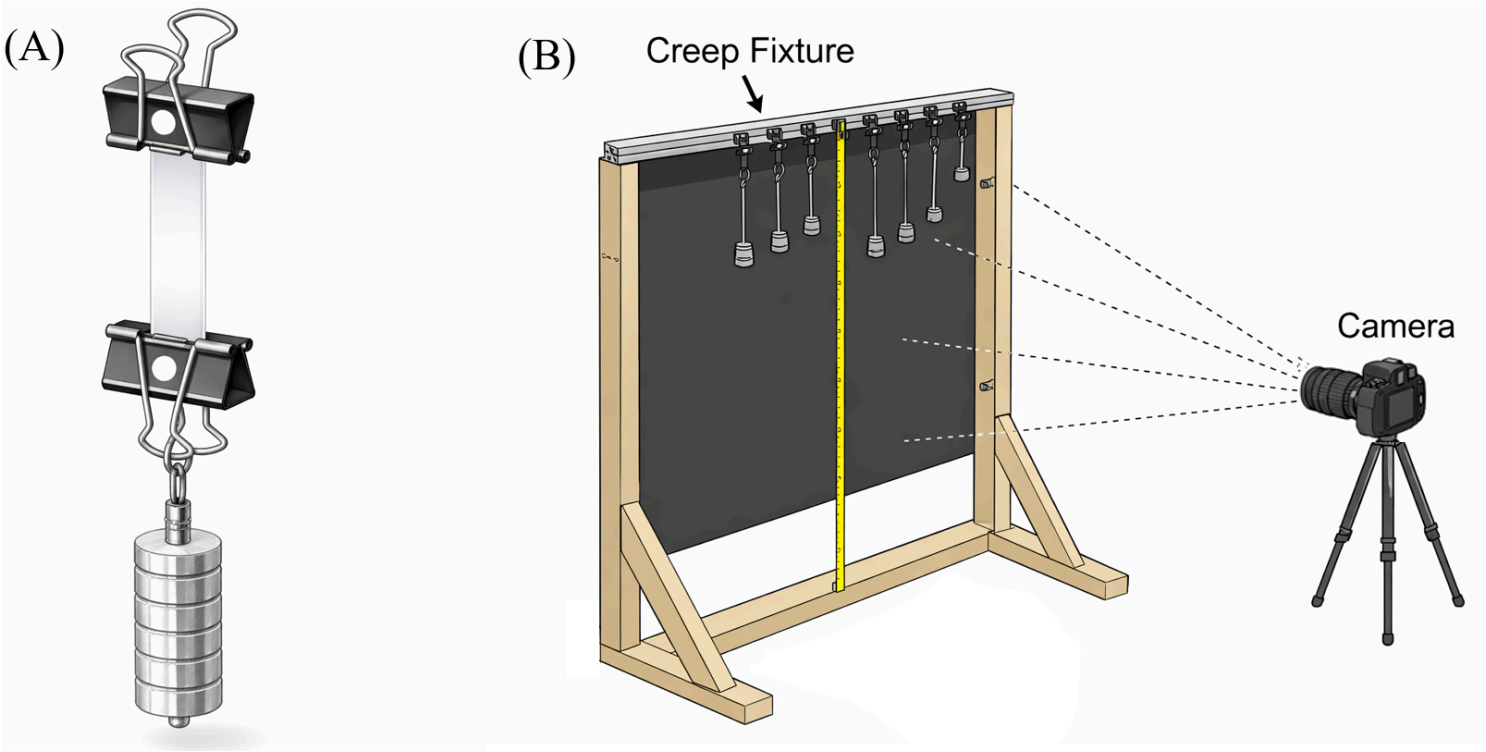


Figure 2

Experimental setup for constant-load creep testing of soft elastomer specimens. (A) Schematic of the specimen configuration, where the elastomer sample is secured between two binder clips and subjected to a constant tensile load via a suspended dead weight. (B) Overview of the custom-built creep fixture and optical tracking system. Multiple specimens are mounted vertically within the frame and loaded by hanging masses, while a camera positioned normal to the sample plane continuously records deformation for displacement tracking and lifetime determination.

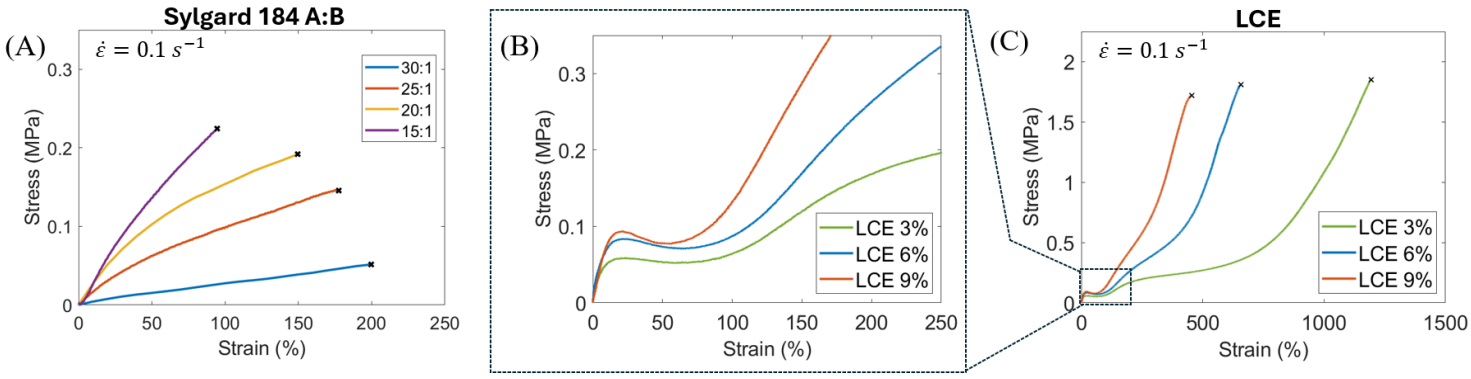


Figure 3

Uniaxial tension of PDMS and LCEs (A) Engineering stress–strain curves of Sylgard 184 prepared at different base-to-curing-agent ratios, tested at a constant strain rate of 0.1 s^{-1}. (B) Low-strain stress–strain response of LCEs with varying crosslink percentages, shown for direct comparison with PDMS

behavior in the small-deformation regime. (C) Full stress–strain curves of LCEs across the complete deformation range for different crosslink percentages.

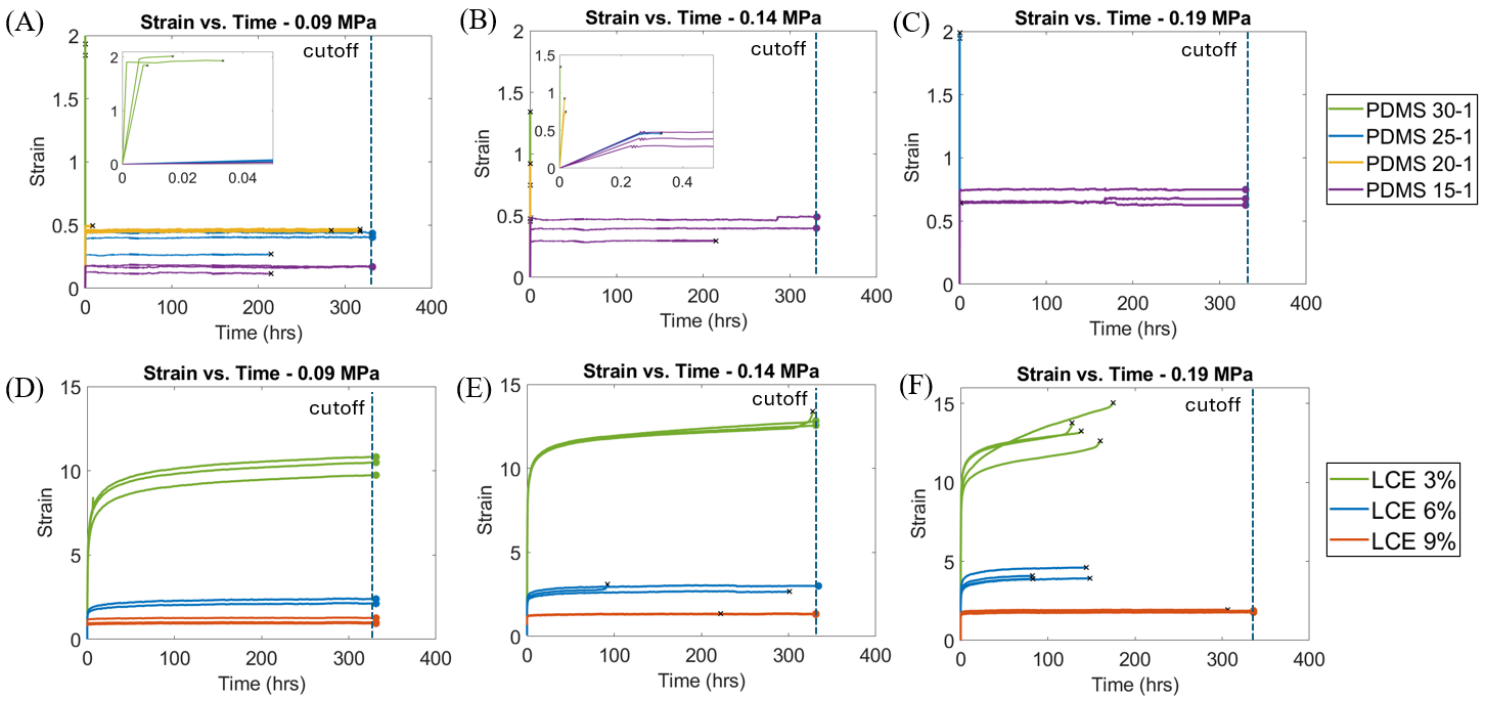


Figure 4

Constant-load creep response of PDMS and LCE networks at applied stresses of 0.09 MPa (A, D), 0.14 MPa (B, E), and 0.19 MPa (C, F). (A–C) Strain-time curves for Sylgard 184 (PDMS) formulated at base-to-curing-agent ratios of 15:1, 20:1, 25:1, and 30:1. (D–F) Strain-time curves for LCE networks with 3%, 6%, and 9% crosslink density. Insets in (A) and (B) highlight the initial deformation regime. Dashed vertical lines indicate the experimental cutoff time.

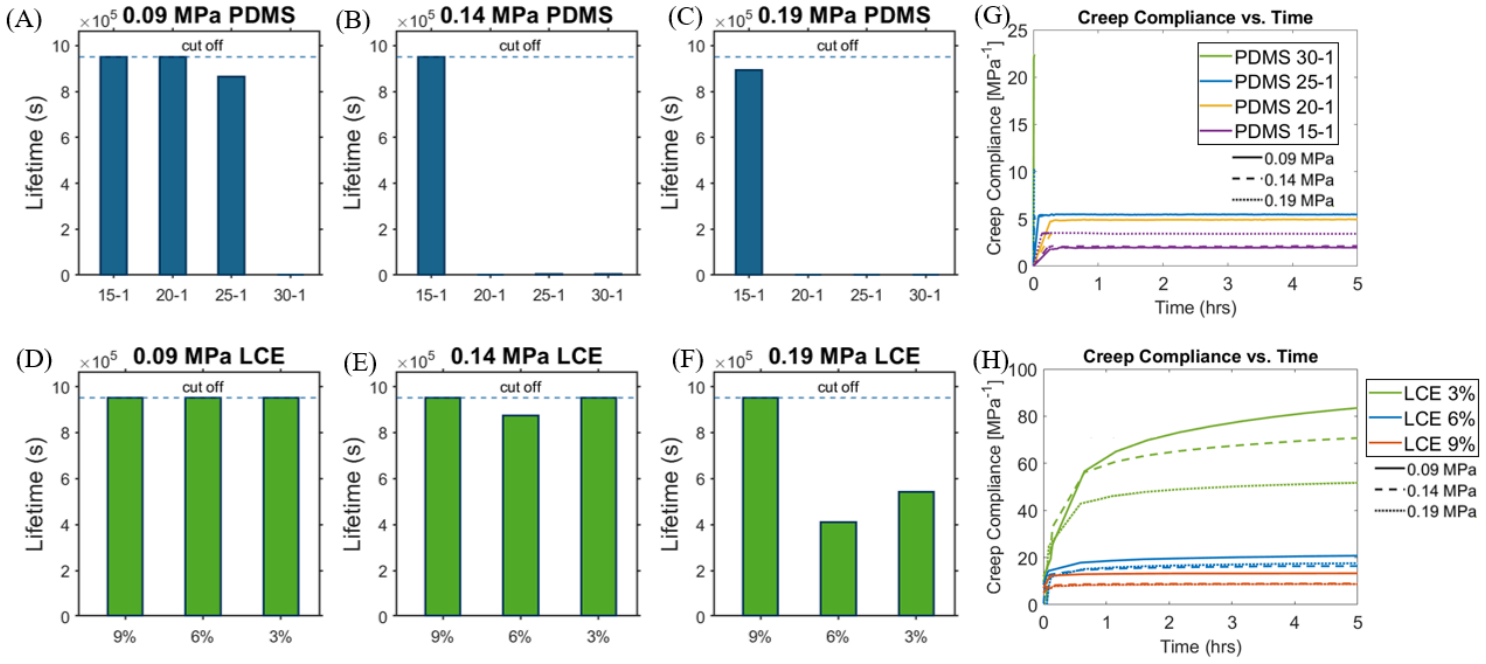


Figure 5

Comparison of creep lifetime and compliance for PDMS and liquid crystal elastomers (LCEs) at multiple applied stresses. (A–C) Creep lifetime of Sylgard 184 (PDMS) prepared at different base-to-curing-agent ratios (15:1, 20:1, 25:1, 30:1) under constant nominal stresses of 0.09 MPa (A), 0.14 MPa (B), and 0.19 MPa (C). (D–F) Creep lifetime of LCE networks with varying crosslink densities (3%, 6%, 9%) under the same applied stresses of 0.09 MPa (D), 0.14 MPa (E), and 0.19 MPa (F). Bars reaching the dashed horizontal line indicate specimens that survived the two-week experimental cutoff without failure and therefore represent lower bounds on creep lifetime. (G) Short-time creep compliance of PDMS formulations under 0.09 MPa (solid lines), 0.14 MPa (dashed lines), and 0.19 MPa (dotted lines). (H) Short-time creep compliance of LCE networks under the same applied stresses (solid: 0.09 MPa; dashed: 0.14 MPa, dotted: 0.19 MPa). Together, the data compare early-time viscoelastic compliance with long-term creep lifetime, highlighting the contrasting stress-dependent durability of conventional PDMS and lightly crosslinked LCE networks.

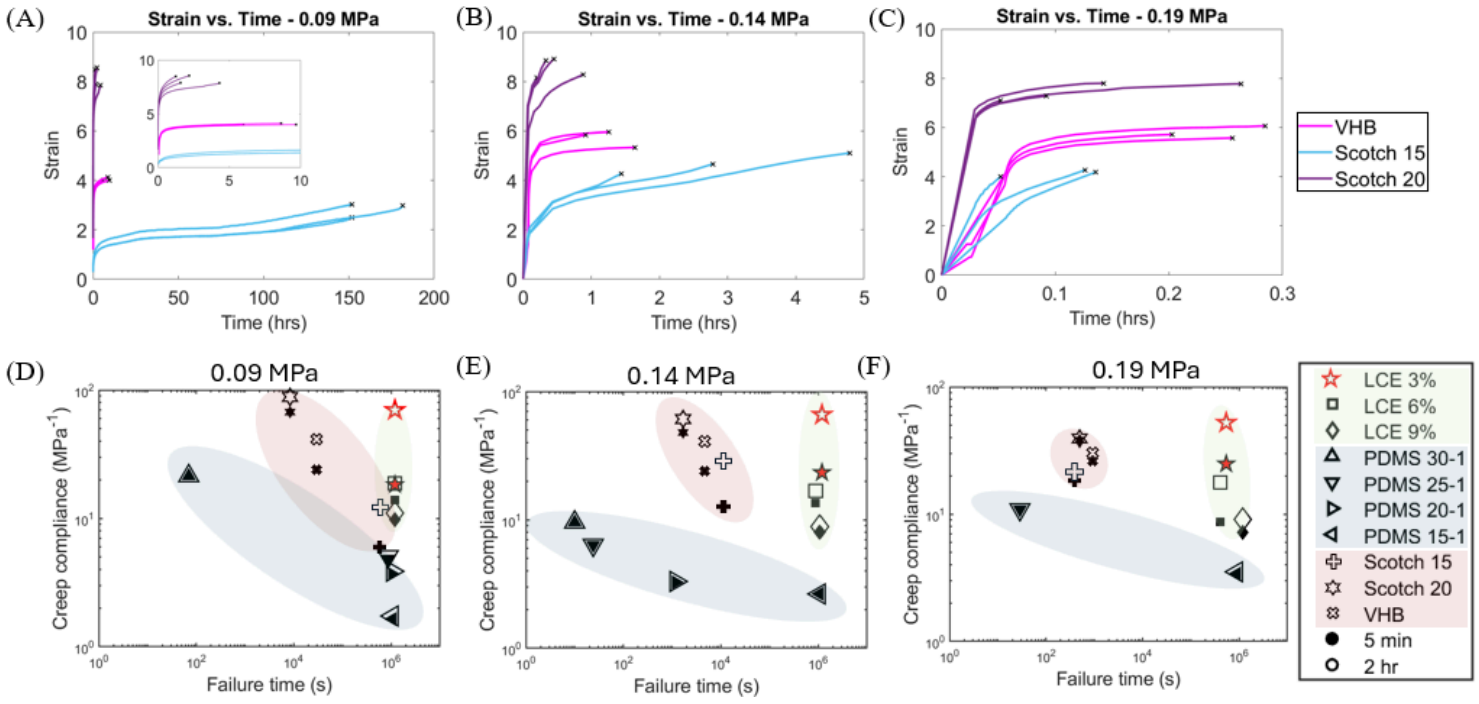


Figure 6

Creep behavior of commercial pressure-sensitive adhesives and compliance–lifetime Ashby plots. (A–C) Constant-load creep strain–time curves for 3M VHB 4910, Scotch 15, and Scotch 20 under applied stresses of 0.09 MPa (A), 0.14 MPa (B), and 0.19 MPa (C). Insets highlight the early-time deformation response. (D–F) Ashby-style plots of creep compliance versus failure time at 0.09 MPa (D), 0.14 MPa (E), and 0.19 MPa (F), comparing commercial PSAs with LCE networks and PDMS formulations. Marker shape denotes material formulation, while the filled and open symbols represent creep compliance measured at 5 min and 2 h, respectively. Shaded regions indicate the approximate property space occupied by each material class. These plots highlight the trade-off between compliance and creep

lifetime and place the commercial PSAs in the context of the model elastomer systems examined here. For the PDMS samples, the 5 min and 2 h markers largely overlap because the compliance changes only weakly over this interval. Points corresponding to specimens that survived the experimental cutoff should be interpreted as lower bounds in failure lifetime.

Supplementary Files

This is a list of supplementary files associated with this preprint. Click to download.

- SILCECreepnpjSoftMatter.docx